Near-Field Rainbow: Wideband Beam Training for XL-MIMO

Mingyao Cui, Linglong Dai, Zhaocheng Wang, Shidong Zhou, and Ning Ge

***Abstract*— Wideband extremely large-scale multiple-input-multiple-output (XL-MIMO) plays an important role in boosting the data rate for 6G networks. Because of the huge bandwidth and the large number of antennas, wideband XL-MIMO introduces a significant near-field beam split effect, where beams at different frequencies are focused on different locations. This effect results in a severe array gain loss, and existing works mainly consider to compensate for this loss by utilizing time-delay (TD) beamforming. This paper demonstrates that despite degrading the array gain, the near-field beam split effect can also contribute to the fast near-field beam training. Specifically, we first reveal the controllable near-field beam split effect. This effect indicates that TD beamforming can control the degree of the near-field beam split effect, i.e., beams at different frequencies can flexibly occupy the desired location range. Due to the similarity with the dispersion of natural light caused by a prism, we also call this effect as "near-field rainbow". Then, by taking advantage of the near-field rainbow, a fast wideband beam training scheme is proposed to generate beams focusing on multiple locations at multiple frequencies with the help of TD beamforming. Finally, simulation results demonstrate that the proposed scheme is able to realize efficient near-field beam training with low training overheads.**

***Index Terms*— XL-MIMO, near-field, wideband, beam training.**

I. Introduction

WIDEBAND extremely large-scale multiple-input-multiple-output (XL-MIMO) has been regarded as a promising technology to meet the capacity requirement for future 6G communications [1], [2]. Benefiting from the large spatial multiplexing gain provided by a very large number of antennas (e.g. 1000+ antennas), XL-MIMO is able to significantly increase the spectrum efficiency [3]. Moreover, XL-MIMO can also provide very high beamforming gain to compensate for the severe path loss at millimeter-wave (mmWave) and terahertz (THz) bands, which may provide tens of GHz-wide bandwidth to enable Tbps data rates for future 6G networks [4].

Due to the very large array aperture and the huge bandwidth at high frequencies, a significant near-field beam split effect will be introduced for wideband XL-MIMO [5]. First, compared to the far-field propagation in previous 1G-5G systems, where radiated electromagnetic (EM) waves can be approximated as *planar* waves, the deployment of XL-MIMO for 6G, especially at high-frequencies, indicates that the near-field propagation will become essential. In the near-field region, the EM waves have to be accurately modeled as *spherical* waves [6], [7]. The boundary between the far-field and near-field regions is determined by the Rayleigh distance, which is proportional to the square of the array aperture and the signal frequency [8]. With the increased array aperture and frequency of wideband XL-MIMO, its near-field range could reach several dozens or even hundreds of meters [7]. For example, for a 1-meter diameter array operating at 30 GHz, the near-field region extends to the distance of 200 meters, dominating a typical 5G cell. As a result, spherical waves should be exploited to realize **near-field beamfocusing** (near-field beamforming) in XL-MIMO systems to focus signals on a *specific location*, rather than the conventional **far-field beam-steering** (far-field beamforming) that steers signals towards a *specific angle* [9], [10].

Second, the very large bandwidth results in the near-field beam split effect. In XL-MIMO systems, the classical frequency-independent phase-shifter (PS) beamforming is naturally considered to generate beams focused on certain locations to provide high beamfocusing gain [11], [12]. This PS beamforming technique works well for narrowband systems. However, for wideband systems, the beams at different frequencies will be focused on different physical locations due to the use of *frequency-independent* PSs. This phenomenon is defined as the **near-field beam split** effect [5], which results in a severe array gain loss, since beams over a large number of frequency subcarriers cannot be aligned with the target user at a certain location. Thus, this near-field beam split effect should be carefully addressed.

A. Prior Works

As the antenna number is not very large for current 5G massive MIMO communications [13], existing works mainly focus on the simplified *far-field beam split* effect [14], [15]. To be specific, the channels are modeled under planar wave assumption, and the beams over different frequencies are split into different spatial angles, where the distance information

Manuscript received 24 May 2022; revised 11 September 2022; accepted 29 October 2022. Date of publication 21 November 2022; date of current version 12 June 2023. The associate editor coordinating the review of this article and approving it for publication was C.-K. Wen. This work was supported in part by the National Key Research and Development Program of China under Grant 2020YFB1807201 and Grant 2018YFB1801102 and in part by the National Natural Science Foundation of China under Grant 62031019. *(Corresponding author: Linglong Dai.)*

The authors are with the Department of Electronic Engineering, Tsinghua University, Beijing 100084, China, and also with the Beijing National Research Center for Information Science and Technology (BNRist), Beijing 100084, China (e-mail: cmy20@mails.tsinghua.edu.cn; daill@tsinghua.edu.cn; zcwang@tsinghua.edu.cn; zhousd@tsinghua.edu.cn; gening@tsinghua.edu.cn).

Color versions of one or more figures in this article are available at https://doi.org/10.1109/TWC.2022.3222198.

Digital Object Identifier 10.1109/TWC.2022.3222198

of spherical wave is ignored. These works can be generally classified into two categories, i.e., techniques overcoming the far-field beam split effect [14], [16], [17], [18], [19], and those taking advantage of it [20], [21], [22]. The first category desires to mitigate the array gain loss caused by the far-field beam split. Various time-delay (TD) beamforming architectures have been studied to achieve this target, such as true-time-delay array [16], [17] and delay-phase precoding structure [14], [19]. Thanks to the *frequency-dependent* phase shift provided by TD beamforming, the generated beams over the entire bandwidth can be aligned with a certain spatial angle, and thus the far-field beam split effect can be alleviated. For the second category of taking advantage of the far-field beam split, it has been proved that TD beamforming can not only mitigate the far-field beam split, but also flexibly control its degree [20], [21], [22]. By carefully designing the delay parameters, the covered angular range of beams over multiple frequencies is controllable. Benefiting from this fact, very fast channel station information (CSI) acquisition in the far-field, such as fast beam training or beam tracking, can be realized. For example, in [20] and [21], fast beam training schemes with only one pilot overhead were studied by utilizing true-time-delay arrays to generat frequency-dependent beams to simultaneously search multiple angles. Moreover, a fast beam tracking scheme based on the delay-phase precoding architecture was proposed in [22] by adaptively adjusting the degree of the far-field beam split according to user mobility. As a result, we can conclude that although far-field beam split results in a severe beamsteering gain loss that should be addressed, it can also benefit the fast far-field CSI acquisition in massive MIMO systems.

When it comes to the XL-MIMO systems, the more realistic near-field beam split effect should be considered, since the antenna number is very large. Specifically, the near-field beam split effect was defined and analyzed in our previous work [5], and TD beamforming was also utilized to overcome this effect. We have proposed to partition the entire array into multiple sub-arrays, and then the user can be assumed to be located within the near-field range of the entire array but in the far-field range of each sub-array. Based on this array partition, TD beamforming can be also exploited to compensate for the group delays across different sub-arrays induced by near-field spherical waves. As a result, the beams over the entire bandwidth can be focused on the desired spatial angle and distance, and the near-field beam split effect is alleviated accordingly.

Efficient wideband XL-MIMO beamfocusing for alleviating the near-field beam split effect requires accurate near-field CSI. To meet this requirement, an intuitive solution is to directly utilize the existing wideband far-field CSI acquisition schemes [20], [21], [22] to estimate the near-field wideband channel. However, since the far-field planar wave assumption mismatches the real near-field spherical wave, these methods [20], [21], [22] may be not valid in the near-field range. To cope with this problem, inspired by the classical far-field hierarchical beam training scheme [23], a near-field hierarchical beam training method was proposed in [24], which uniformly searches multiple angles and distances to obtain the near-field CSI. Moreover, from the perspective of near-field array gain, [6] proved that the distances should be non-uniformly searched for improving channel estimation accuracy. Nevertheless, existing near-field CSI acquisition methods [6], [24], [25] assume that the bandwidth is not very large, so the near-field beam split effect has not been considered. Moreover, unlike the angle-dependent far-field CSI, to obtain the near-field CSI, the angle and distance information should be estimated simultaneously, which may result in unacceptable pilot overhead for near-field beam training [24]. Unfortunately, to the best of our knowledge, how to accurately obtain wideband XL-MIMO near-field CSI with acceptable pilot overhead has not been studied in the literature.

B. Our Contributions

To fill in this gap, inspired by the two categories of research on the far-field beam split, i.e., overcoming and taking advantage of it, we unveil that although the near-field beam split effect degrades the array gain, it can also provide a new possibility to speed up the near-field CSI acquisition. Based on this new finding, we propose a fast wideband near-field beam training scheme by taking advantage of the near-field beam split effect. Specifically, our contributions are summarized as follows.

- Firstly, we prove the controllable effect of near-field beam split, i.e., TD beamforming can flexibly control the degree of near-field beam split. Specifically, it has been proved that, in far-field scenarios, TD beamforming can control the covered angular range of beams over multiple frequencies when the distance is very large [20], [21], [22]. By contrast, we will reveal the phenomenon that not only the covered angular range, but also the covered distance range of beams over different frequencies are controllable by the elaborate design of TD parameters. This phenomenon implies that the manipulation of the near-field beam split is achievable. A simple analogy of the controllable near-field beam split effect is the dispersion of white light with a large bandwidth caused by a prism. Thereby in this paper, this effect is also termed as "**near-field rainbow**". The near-field rainbow effect allows us to generate multiple beams focused on multiple locations simultaneously by TD beamforming, which is unachievable by the classical PS beamforming.
- Then, based on the mechanism of near-field rainbow, a wideband near-field beam training scheme is proposed to realize fast near-field CSI acquisition. In the proposed scheme, multiple beams focused on multiple angles in a given distance range are generated by TD beamforming in each time slot. Next, in different time slots, different distance ranges are measured by fine-tuning the time-delay parameters. In this way, the optimal spatial angle can be searched in a frequency-division manner, while the optimal distance is obtained in a time-division manner. Unlike the exhaustive near-field beam training scheme that searches only one location in each time slot, the proposed scheme is able to search multiple locations in each time slot. Thus, the near-field rainbow based beam training can be significantly reduce the pilot overhead.

- Finally, we analyze the training overhead and the maximum delay range of the proposed method. We also provide simulation results to demonstrate the mechanism of near-field rainbow and verify the advantages of the proposed beam training scheme. We demonstrate that our scheme is able to achieve a satisfactory average rate performance with a significantly reduced training overhead. We also show that our beam training approach outperforms the existing far-field schemes in the near-field range. Additionally, our scheme also works well in the far-field range, since the proposed near-field beam training scheme is able to automatically decay to the far-field beam training in the far-field environments.[1]

C. Organization and Notation

1) Organization: The rest of this paper is organized as below. In Section II, the system model is introduced. We first explain the near-field beam split effect in wideband XL-MIMO systems and then discuss how to mitigate it using TD beamforming. Then in Section III, we prove the mechanism of controllable near-field beam split. In Section IV, the exhaustive near-field beam training is defined and the near-field rainbow based beam training is proposed. Section V provides the simulation results. Finally, conclusions are drawn in Section VI.

2) Notation: Lower-case and upper-case boldface letters represent vectors and matrices, respectively; $[\mathbf{x}]_n$ denotes the n-th element of the vector $\mathbf{x}$; $(\cdot)^*$, $(\cdot)^T$, and $(\cdot)^H$ denote the conjugate, transpose, and conjugate transpose, respectively; $|\cdot|$ and $\mathrm{Tr}(\cdot)$ denote the absolute and trace operator; $\lceil x \rceil$ denotes the nearest integer greater than or equal to x; $\mathcal{CN}(\mu, \Sigma)$ and $\mathcal{U}(a, b)$ denote the Gaussian distribution with mean μ and covariance Σ, and the uniform distribution between a and b, respectively.

II. System Model

In this section, we first introduce the near-field wideband channel model, and then explain the near-field beam split effect in wideband XL-MIMO. Finally, we discuss how to mitigate the near-field beam split effect by using TD beamforming.

A. Near-Field Wideband Channel Model

We consider a wideband XL-MIMO communication system in this paper. The base station (BS) is equipped with a uniform-linear-array (ULA) to serve a single omnidirectional antenna user using orthogonal frequency division multiplexing (OFDM) with M subcarriers. For expression simplicity, we assume the number of BS antennas is $N_t = 2N + 1$. We denote B, c, f_c, $\lambda_c = \frac{c}{f_c}$ as the bandwidth, the light speed, the central carrier frequency, and the central wavelength, respectively. The antenna spacing is presented as $d = \frac{\lambda_c}{2}$.

Due to the severe path loss incurred by the scatters, mmWave and THz communications heavily rely on the line-of-sight (LoS) path [4]. Therefore, we mainly focus on the near-field LoS channel, while the discussions in this paper can be straightforwardly extended to the non-LoS (NLoS) scenarios. As shown in Fig. 1, the user is located at $(r_0 \cos\vartheta_0, r_0 \sin\vartheta_0)$ with $\theta_0 = \sin\vartheta_0$. Taking into account the near-field spherical wave characteristic [26], the channel between the n-th BS antenna and the user at the m-th subcarrier with $n = \{-N, \cdots, 0, \cdots, N\}$ and $m = \{1, 2, \cdots, M\}$ can be represented as

$$[\mathbf{h}_m]_n = \beta_m^{(n)} e^{-jk_m r_0^{(n)}}, \tag{1}$$

where $k_m = \frac{2\pi f_m}{c}$ denotes the wavenumber at subcarrier frequency $f_m = f_c + \frac{B}{M}\left(m - 1 - \frac{M-1}{2}\right)$, and $r_0^{(n)}$ represents the distance between the user and the n-th BS antenna. As the coordinate of the n-th BS antenna is $(0, nd)$, $r_0^{(n)}$ can be derived from geometrical relationship as $r_0^{(n)} = \sqrt{(r_0\cos\vartheta_0)^2 + (r_0\sin\vartheta_0 - nd)^2} = \sqrt{r_0^2 + n^2d^2 - 2r_0\theta_0 nd}$. The free-space path gain $\beta_m^{(n)}$ can be modeled as [27]

$$\beta_m^{(n)} = \frac{\lambda_m}{4\pi r_0^{(n)}}, \tag{2}$$

where $\lambda_m = \frac{f_m}{c}$ denotes the wavelength. Generally, the distance r_0 between the user and BS is larger than the array aperture $D = (N_t - 1)d$. For example, for a 256-element ULA working at 30 GHz, r_0 is very likely to be larger than $D = 255 \times 0.5 \times 10^{-3} = 1.275$ meters. With $r_0 > D$, we can assume $\beta_m^{(-N)} \approx \cdots \approx \beta_m^{(N)} \approx \beta_m = \frac{\lambda_m}{4\pi r_0}$ based on the Fresnel approximation [28]. As a result, the near-field LoS channel $\mathbf{h}_m \in \mathbb{C}^{N_t \times 1}$ can be represented as

$$\begin{aligned}\mathbf{h}_m &= \beta_m \left[e^{-jk_m r_0^{(-N)}}, \cdots, e^{-jk_m r_0^{(N)}}\right]^T \\ &= \sqrt{N_t}\beta_m \mathbf{a}_m(\theta_0, r_0),\end{aligned} \tag{3}$$

where $\mathbf{a}_m(\theta_0, r_0)$ is the near-field array response vector. Notice that since the near-field spherical wave characteristic is considered, the array response vector $\mathbf{a}_m(\theta_0, r_0)$ is significantly different from the classical far-field array response vector [29], where the latter is based on the planar wave assumption and ignores the influence of distance r_0. The radius of the near-field region is determined by the Rayleigh distance $\mathrm{RD} = \frac{2D^2}{\lambda_c}$ [8], [30]. For a 1-meter diameter array operating at 30 GHz, its Rayleigh distance reaches up to

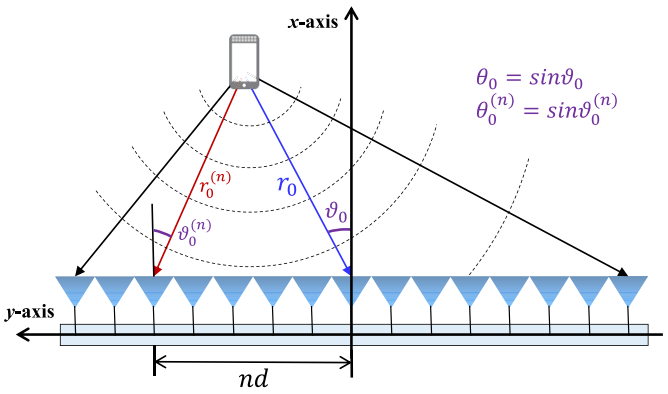

Fig. 1. The near-field channel based on the accurate spherical wave model.

[1]Simulation codes are provided to reproduce the results in this paper: http://oa.ee.tsinghua.edu.cn/dailinglong/publications/publications.html.

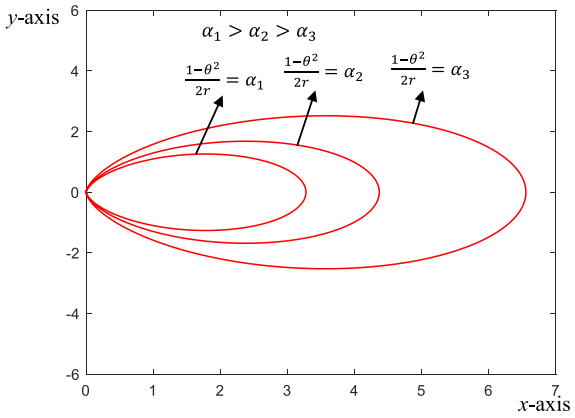

Fig. 2. The schematic diagrams of different distance rings. In this figure, each ring $\alpha = \frac{1-\theta^2}{2r}$ is represented by a red line in the xy-plane (Cartesian Coordinates). The relationship between (r, θ) and (x, y) is $r = \sqrt{x^2+y^2}$ and $\theta = \frac{y}{\sqrt{x^2+y^2}}$, thus the curve $\alpha = \frac{1-\theta^2}{2r}$ is also equivalent to $\alpha = \frac{x^2}{2(x^2+y^2)^{\frac{3}{2}}}$.

200 meters. Therefore, in such a mmWave XL-MIMO system, the near-field spherical wave characteristic becomes essential and the distance information cannot be ignored [31].

However, since the distance $r_0^{(n)}$ is a complicated radical function with respect to the antenna index n, it is difficult to analyze the property of the near-field spherical wave directly from (3). To deal with this problem, the Fresnel approximation [28] can be adopted to approximate $r_0^{(n)}$ as

$$r_0^{(n)} \overset{(a)}{\approx} r_0 - nd\theta_0 + n^2 d^2 \frac{1-\theta_0^2}{2r_0}, \tag{4}$$

where (a) is based on the second-order Taylor expansion $\sqrt{1+x} \approx 1 + \frac{1}{2}x - \frac{1}{8}x^2$. For expression simplicity, we denote $\alpha_0 = \frac{1-\theta_0^2}{2r_0}$ and $\alpha = \frac{1-\theta^2}{2r}$. As shown in Fig. 2, the curve $\alpha = \frac{1-\theta^2}{2r}$ corresponds to a ring in the physical space. Thereby, we call the curve $\alpha = \frac{1-\theta^2}{2r}$ the *distance ring* α. Then, according to (4), the n-th element of $\mathbf{a}_m(\theta_0, r_0)$ can be approximated as

$$\begin{aligned}[\mathbf{a}_m(\theta_0, r_0)]_n &\approx \frac{1}{\sqrt{N_t}} e^{-jk_m(r_0 - nd\theta_0 + n^2 d^2 \alpha_0)} \\ &= e^{-jk_m r_0} [\mathbf{b}_m(\theta_0, \alpha_0)]_n,\end{aligned} \tag{5}$$

where $[\mathbf{b}_m(\theta_0, \alpha_0)]_n = \frac{1}{\sqrt{N_t}} e^{jk_m(nd\theta_0 - n^2 d^2 \alpha_0)}$ denotes the n-th element of vector $\mathbf{b}_m(\theta_0, \alpha_0)$. Since the constant phase $e^{-jk_m r_0}$ in (5) is independent of the antenna index n, we only need to discuss the vector $\mathbf{b}_m(\theta_0, \alpha_0)$.

B. Near-Field Beam Split

At mmWave or THz band, *frequency-independent* PS beamforming is widely considered to generate a focused beam aligned with the user location (r_0, θ_0) in the polar coordinate. The beamfocusing vector $\mathbf{w}_{\text{PS}}$ generated by frequency-independent PSs is usually set as $\mathbf{w}_{\text{PS}} = \mathbf{b}_c^*(\theta_0, \alpha_0)$, in order to focus the beam energy on the location (r_0, θ_0) [9]. Here, $\mathbf{b}_c(\theta_0, \alpha_0)$ represents the array response vector (5) at frequency f_c.

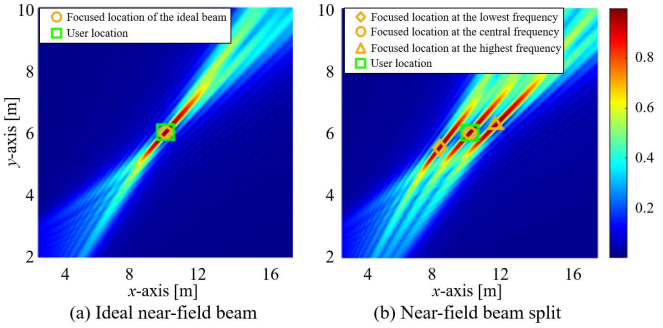

(a) Ideal near-field beam (b) Near-field beam split

Fig. 3. The schematic diagram of the near-field beam split effect. The center of the BS's antenna array is regarded as the x-y coordinate origin and the user location is $(10\,\text{m}, 6\,\text{m})$. Sub-figure (a) indicates for efficient data transmission, the ideal beams over all frequencies should be focused on the target user location. However, sub-figure (b) illustrates that due to the near-field beam split effect, only beams around the central frequency generated by PS beamforming can be aligned with the target user location, while others are separated from this location. For expression clarity, we only plot three subcarriers here.

However, the array response vectors (5) of wideband channels are *frequency-dependent*, which mismatches the *frequency-independent* beamfocusing vector $\mathbf{w}_{\text{PS}} = \mathbf{b}_c^*(\theta_0, \alpha_0)$. This mismatch leads to the fact that, the beams generated by $\mathbf{w}_{\text{PS}}$ at different frequencies will be focused on different locations, which is detailed in the following **Lemma 1**.

Lemma 1: For near-field wideband communications, the beam at frequency f_m generated by $\mathbf{w}_{PS} = \mathbf{b}_c^*(\theta_0, \alpha_0)$ will be focused on the location (θ_m, r_m), satisfying

$$\theta_m = (k_c/k_m)\theta_0 = (f_c/f_m)\theta_0 = \theta_0/\eta_m, \tag{6}$$

$$\alpha_m = (k_c/k_m)\alpha_0 = (f_c/f_m)\alpha_0 = \alpha_0/\eta_m, \tag{7}$$

where we define $\alpha_m = \frac{1-\theta_m^2}{2r_m}$, $\eta_m = f_m/f_c$, and $k_c = \frac{2\pi f_c}{c}$.

Proof: At frequency f_m, the array gain achieved by $\mathbf{w}_{\text{PS}}$ on an arbitrary user location (r, θ) with $\alpha = \frac{1-\theta^2}{2r}$ is

$$\begin{aligned}|\mathbf{w}_{\text{PS}}^T \mathbf{b}_m(\theta, \alpha)| &= \frac{1}{N_t} \left| \sum_{n=-N}^{N} e^{jnd(k_m\theta - k_c\theta_0) - jn^2 d^2 (k_m \alpha - k_c \alpha_0)} \right| \\ &= G(k_m\theta - k_c\theta_0, k_m\alpha - k_c\alpha_0),\end{aligned} \tag{8}$$

where we define $G(x, y) = \frac{1}{N_t} \left| \sum_n e^{jndx - jn^2 d^2 y} \right|$. Apparently, the beam at frequency f_m is focused on the location (r_m, θ_m) corresponding to the maximum array gain, i.e.,

$$(r_m, \theta_m) = \arg\max_{r,\theta} G(k_m\theta - k_c\theta_0, k_m\alpha - k_c\alpha_0), \tag{9}$$

where $\alpha_m = \frac{1-\theta_m^2}{2r_m}$. Since $G(0,0) = 1$ and $|G(x,y)| \le 1$, it is obvious that $(x, y) = (0, 0)$ is an optimal solution to maximize the function $G(x, y)$. Therefore, we have $k_m\theta_m - k_c\theta_0 = 0$ and $k_m\alpha_m - k_c\alpha_0 = 0$, which gives rise to the results of (6) and (7). ■

According to **Lemma 1**, the beam at f_m is focused on the location $(\theta_m, r_m) = (\theta_m, \frac{1-\theta_m^2}{2\alpha_m}) = (\frac{\theta_0}{\eta_m}, r_0 \frac{\eta_m - \frac{1}{\eta_m}\theta_0^2}{1-\theta_0^2})$. As shown in Fig. 3, since the desired user is located at $(r_0, \theta_0) \neq (r_m, \theta_m)$, the beam at frequency f_m cannot be aligned with the desired user location. This misalignment is termed as the "near-field beam split" effect [5], which will

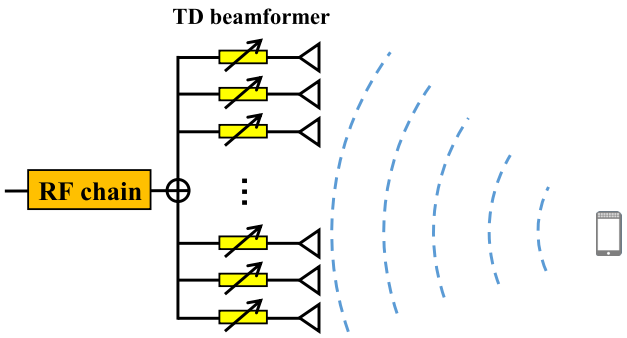

Fig. 4. The TD beamforming architecture.

result in a severe array gain loss when f_m is far away from f_c in wideband XL-MIMO systems. For example, if the carrier frequency and bandwidth are 30 GHz and 1 GHz, and the BS is equipped with a 256-element ULA, then around 50% of subcarriers will suffer from more than 50% array gain loss [5]. Therefore, the near-field beam split effect should be elaborately addressed, especially when the bandwidth is very large.

C. Time-Delay Beamforming

To mitigate the near-field beam split effect, one can harness TD beamforming rather than PS beamforming to generate frequency-dependent beams to match the frequency-dependent channels. Notice that TD beamsteering has been studied in far-field wideband communications [14], [16], [17], [18], [19], [20], [21], [22], while in this study, we consider utilizing it to overcome and control the near-field beam split effect.

As shown in Fig. 4, we assume the BS is equipped with an N_t-element TD beamforming architecture, where each antenna is connected to one time-delay circuit. Time-delay circuits have various implementations, such as analog delay lines [32], digital delay circuits [14], and analog baseband delay lines [21]. By manipulating the delay in each antenna branch, each TD circuit is capable of tuning frequency-dependent phase shifts on wideband signals. Mathematically speaking, we denote $\tau^{(n)'}$ as the adjustable delay of the n-th TD circuit. Its time-domain response is $\delta(t-\tau^{(n)'})$ with $\delta(t)$ being the impulse function. Then, the corresponding frequency-domain response at f_m is $e^{-j2\pi f_m \tau^{(n)'}}$. Consequently, we can use $\mathbf{w}_m$ to represent the TD beamforming vecto. By considering the normalized power constraint, the n-th element of $\mathbf{w}_m$ is $[\mathbf{w}_m]_n = \frac{1}{\sqrt{N_t}} e^{-j2\pi f_m \tau^{(n)'}}$. For expression clarity, we denote $r^{(n)'} = c\tau^{(n)'}$ and then $[\mathbf{w}_m]_n$ becomes $\frac{1}{\sqrt{N_t}} e^{-jk_m r^{(n)'}}$. Notice that $[\mathbf{w}_m]_n$ has a similar form to the array response vector $[\mathbf{b}_m(\theta_0, r_0)]_n = \frac{1}{\sqrt{N_t}} e^{jk_m(nd\theta_0 - n^2 d^2 \alpha_0)}$. Thus, we set $r^{(n)'}$ as

$$r^{(n)'} = nd\theta' - n^2 d^2 \alpha', \tag{10}$$

where θ' and α' are defined as the adjustable TD parameters. Accordingly, the beamfocusing vector at f_m can be presented as

$$[\mathbf{w}_m(\theta', \alpha')]_n = \frac{1}{\sqrt{N_t}} e^{-jk_m(nd\theta' - n^2 d^2 \alpha')}. \tag{11}$$

In this case, at frequency f_m, the array gain on an arbitrary location (r, θ) with $\alpha = \frac{1-\theta^2}{2r}$ is given by

$$\begin{aligned} &|\mathbf{w}_m(\theta', \alpha')^T \mathbf{b}_m(\theta, \alpha)| \\ &= \frac{1}{N_t} \left| \sum_{n=-N}^{N} e^{jnd(k_m\theta - k_m\theta') - jn^2 d^2 (k_m\alpha - k_m\alpha')} \right| \\ &= G(k_m(\theta - \theta'), k_m(\alpha - \alpha')). \end{aligned} \tag{12}$$

Obviously, the beam at f_m is focused on $(r_m, \theta_m) = \arg\max_{r,\theta} G(k_m(\theta - \theta'), k_m(\alpha - \alpha'))$. Similar to the derivation of the optimal solution of (9), $G(k_m(\theta - \theta'), k_m(\alpha - \alpha'))$ approaches its maximum value when $k_m(\theta - \theta') = 0$ and $k_m(\alpha - \alpha') = 0$. Therefore, the beam at frequency f_m is focused on $\theta_m = \theta'$ and $r_m = r' = \frac{1-\theta'^2}{2\alpha'}$, which is independent of f_m. Then, once the LoS path information (r_0, θ_0) is available at the BS and the TD parameters are set as $\theta' = \theta_0$ and $\alpha' = \frac{1-\theta_0^2}{2r_0}$, then the beams across the entire bandwidth are able to be focused on the location $\theta_m = \theta' = \theta_0$ and $r_m = \frac{1-\theta'^2}{2\alpha'} = r_0$. As a consequence, the near-field beam split effect can be mitigated by TD beamforming.

On the other hand, efficient wideband beamfocusing requires that the LoS path information (r_0, θ_0) is available at the BS side. To meet this requirement, in the following discussions, we prove that TD beamforming can not only mitigate the near-field beam split effect, but also flexibly control its degree. Then, we will further utilize this property to achieve efficient near-field beam training to obtain (r_0, θ_0).

III. Mechanism of Controllable Near-Field Beam Split

In [20], [22], and [21], the mechanism of controllable far-field beam split has been proved, i.e., by elaborately designing the time-delay parameters, beams over the entire bandwidth are able to cover a desired angular range in the far-field. By taking advantage of this mechanism, multiple beams aligned with multiple angles can be generated by only one radio-frequency (RF) chain to acquire the far-field CSI rapidly. Similarly, to obtain the near-field CSI, we surprisingly find that TD beamforming can not only control the angular coverage range but also control the distance coverage range of the beams, i.e., the controllable near-field beam split is achievable. In this section, for better understanding, we will prove the controllable far-field beam split at first, and then extend it to the near-field scenarios.

A. Controllable Far-Field Beam Split

In far-field scenarios, the distances r and r' are assumed to be larger than the Rayleigh distance RD, so that the spherical wave can be approximated as a planar wave. In this case, all of the distance-related parameters $\alpha = \frac{1-\theta^2}{2r}$ and $\alpha' = \frac{1-\theta'^2}{2r'}$ reliably approach 0. Then, the array response vector becomes $[\mathbf{b}_m(\theta, \alpha)]_n = [\mathbf{b}_m(\theta, 0)]_n = \frac{1}{\sqrt{N_t}} e^{jk_m nd\theta}$, and the beamfocusing vector realized by TD beamforming becomes $[\mathbf{w}_m(\theta', 0)]_n = \frac{1}{\sqrt{N_t}} e^{-jk_m nd\theta'}$. Therefore, the array

gain in (12) can be simplified as

$$G\left(k_m(\theta-\theta'),0\right)=\left|\frac{\sin\left(\frac{N_t}{2}dk_m(\theta-\theta')\right)}{N_t\sin\left(\frac{1}{2}dk_m(\theta-\theta')\right)}\right|, \quad (13)$$

where $G(x,0)=\left|\frac{\sin\left(\frac{N_t}{2}dx\right)}{N_t\sin\left(\frac{1}{2}dx\right)}\right|$. It has been previously proved that the beams over the entire bandwidth generated by $\mathbf{w}_m(\theta',0)$ are focused on the spatial angle $\theta_m=\theta'$, with $m=1,2,\cdots,M$. However, notice that the spatial angle θ_m is corresponding to an actual physical angle $\vartheta_m=\arcsin\theta_m$ as shown in Fig. 1, which implies the range of θ_m is restrained by $\theta_m\in[-1,1]$. By contrast, θ' is an adjustable parameter of the TD beamforming. A question naturally arises that, if the adjustable parameter is set as $\theta'\notin[-1,1]$, then what does it have to do with the actual spatial angle θ_m? In fact, the answer to this question is exactly the mechanism of the far-field controllable beam split.

For expression simplicity, parameter $\theta'\notin[-1,1]$ is termed as the abnormal value, while parameter $\theta'\in[-1,1]$ is termed as the actual value. Restrained by the range of θ_m, if θ' is an abnormal value, it is obvious that $\theta_m\neq\theta'$. To acquire the relationship between θ_m and θ', we observe that the far-field array gain $G(x,0)$ is a periodic function against x with a period $\frac{2\pi}{d}$. For any integer $p\in\mathbb{Z}$, we have

$$G\left(x-\frac{2p\pi}{d},0\right)=\left|\frac{\sin\left(\frac{N}{2}dx-Np\pi\right)}{N\sin\left(\frac{1}{2}dx-p\pi\right)}\right|=\left|\frac{\sin\left(\frac{N}{2}dx\right)}{N\sin\left(\frac{1}{2}dx\right)}\right| =G(x,0). \quad (14)$$

In Section II, we have indicated that the optimal solution x^{opt} to maximize $G(x,0)$ is $(x^{\text{opt}},0)=(0,0)$. However, according to (14), we find that $(0,0)$ is just one of the optimal solutions for maximizing $G(x,0)$. The periodicity of $G(x,0)$ implies that the optimal solutions should satisfy $(x^{\text{opt}},0)=(\frac{2p\pi}{d},0)$, $p\in\mathbb{Z}$. As a consequence, by solving $\theta_m=\arg\max_\theta G(k_m(\theta-\theta'),0)$, the focused spatial angle θ_m at frequency f_m is derived as

$$\theta_m=\theta'+\frac{2p\pi}{dk_m}=\theta'+\frac{2p}{\eta_m}, \quad (15)$$

where the function of $p\in\mathbb{Z}$ is to ensure $\theta_m\in[-1,1]$ becomes an actual spatial angle. From (15), the mechanism of the controllable far-field beam split is acquired, which has the following features.

Feature 1: Since p is an integer, if $p\neq0$, the spatial angle θ_m is related to the frequency f_m, which means beams at different frequencies will split towards different spatial angles. Therefore, despite the use of TD beamsteering, the far-field beam split effect can also be induced.

Feature 2: The specific value of $p\in\mathbb{Z}$ is determined by θ'. If $\theta'\in[-1,1]$ belongs to the actual value range of θ_m, then p can be zero and θ_m exactly equals to θ'. That is to say, with $\theta'\in[-1,1]$, the far-field beam split effect is eliminated. While if $\theta'\notin[-1,1]$ becomes an abnormal value, then to guarantee that θ_m is an actual spatial angle, it is obvious that p cannot be zero. For instance, if θ' is set as 1.5, at the central frequency f_c with $\eta_c=\frac{f_c}{f_c}=1$, the corresponding spatial angle is $\theta_c=1.5+2p/\eta_c=1.5+2p$, $p\in\mathbb{Z}$. Only if $p=-1$ can $\theta_c=-0.5\in[-1,1]$ be an actual spatial angle. Therefore, with $\theta'\notin[-1,1]$, p is not zero and thus θ_m is a function of the frequency f_m, where the beam split effect is induced again.

Feature 3: Notice that the beam split pattern (15) of TD beamforming is different from the pattern (6) induced by PS beamforming. For PS beamforming cases, the degree of beam split is fixed and uncontrollable. However, TD beamforming allows us to control the degree of beam split by adjusting θ'. For instance, considering the central frequency f_c, if θ' is set as 1.5, then p should be -1 and $\theta_c=1.5-2=-0.5$. On the other hand, if θ' is set as 3.5, then p should be -2 and $\theta_c=3.5-4=-0.5$. For the above two examples, although the spatial angles θ_c are the same, the integers p are different, which indicates the degree of the beam split $\theta_m=\theta'+2p/\eta_m$ is different. Therefore, by adjusting the delay parameter θ', the integer p is indirectly controlled, then the degree of beam split is adjusted. This property is termed as the controllable far-field beam split. Benefiting from this property, the adjustment on the angular coverage range of the beams is achieved, which can be utilized to realize fast far-field CSI acquisition [20], [21], [22].

In the next sub-section, we will extend this conclusion to a more general near-field scenario.

B. Controllable Near-Field Beam Split

For the near-field scenario, the distances r and r' are lower than the Rayleigh distance. Then α and α' can not be zero, and the near-field spherical wave characteristics should be considered. To prove the mechanism of the controllable near-field beam split, similar to the derivation in the far-field scenarios, we consider the abnormal values for the adjustable parameters θ' and α' in (11) simultaneously.

Specifically, it has been discussed before that $\theta'\notin[-1,1]$ is an abnormal value for the angle. As for the distance-related parameter $\alpha=\frac{1-\theta^2}{2r}$, since $1>\theta^2$ and $r>0$, a realistic α should be larger than zero. On this condition, $\alpha'<0$ is the abnormal value for the distance ring. If $\theta'\in[-1,1]$ and $\alpha'>0$ are actual values, it was proved in Section II-C that the near-field beam split effect is eliminated, i.e., beams are focused on $\theta_m=\theta'$ and $\alpha_m=\alpha'$ for all frequencies f_m. On the other hand, for the abnormal value $\theta'\notin[-1,1]$ or $\alpha'<0$, the following **Lemma 2** explains the behaviors of the beams generated by $\mathbf{w}_m(\theta',\alpha')$.

Lemma 2: If $\theta'\notin[-1,1]$ or $\alpha'<0$, the beam at frequency f_m generated by $\mathbf{w}_m(\theta',\alpha')$ according to (11) will be focused on the location (θ_m,r_m), satisfying

$$\theta_m=\theta'+\frac{2p\pi}{dk_m}=\theta'+\frac{2p}{\eta_m}, \quad (16)$$

$$\alpha_m=\alpha'+\frac{2q\pi}{d^2k_m}=\alpha'+\frac{2q}{d\eta_m}, \quad (17)$$

where $r_m=\frac{1-\theta_m^2}{2\alpha_m}$ and $p,q\in\mathbb{Z}$ are integers to guarantee $\theta_m\in[-1,1]$ and $\alpha_m>0$.

Proof: Similar to the derivation of (15), the periodicity of the near-field array gain function $G(x,y)$ should be considered. It is proved in Appendix A that $G(x,y)$ is a

periodic function against the vector variable (x, y) with a period $(\frac{2\pi}{d}, \frac{2\pi}{d^2})$. Therefore, for any integers $p \in \mathbb{Z}$ and $q \in \mathbb{Z}$, $G(x, y)$ can be rewritten as

$$G(x, y) = G(x - \frac{2p\pi}{d}, y - \frac{2q\pi}{d^2}). \tag{18}$$

We have indicated in Section II that the optimal solution $(x^{\text{opt}}, y^{\text{opt}})$ to maximize the array gain $G(x, y)$ is $(x^{\text{opt}}, y^{\text{opt}}) = (0, 0)$. The periodicity in (18) implies $(0, 0)$ is just one of the optimal solutions for maximizing $G(x, y)$. In fact, these solutions should satisfy $(x^{\text{opt}}, y^{\text{opt}}) = (\frac{2p\pi}{d}, \frac{2q\pi}{d^2})$ with $p \in \mathbb{Z}$ and $q \in \mathbb{Z}$. Accordingly, to obtain the focused location of the beam at frequency f_m by solving $(\theta_m, r_m) = \arg\max_{\theta,r} G(k_m(\theta-\theta'), k_m(\alpha-\alpha'))$, we have $k_m(\theta_m-\theta') = \frac{2p\pi}{d}$ and $k_m(\alpha_m - \alpha') = \frac{2q\pi}{d^2}$. As a consequence, θ_m and α_m become $\theta' + \frac{2p}{\eta_m}$ and $\alpha' + \frac{2q}{d\eta_m}$, respectively, where the function of integers p and q is to ensure that $\theta_m \in [-1, 1]$ and $\alpha_m > 0$. ■

According to **Lemma 2**, the mechanism of the controllable near-field beam split is acquired, which has the following features.

Feature 1: If $p \neq 0$ or $q \neq 0$, then θ_m or α_m is dependent on frequency f_m, which implies beams at different frequencies are focused on different locations. Therefore, despite the employment of TD beamforming, the near-field beam split effect can also be induced.

Feature 2: As the function of the abnormal value of θ' has been discussed in the previous section, we mainly explain the impact of the abnormal value of α' on the integer q here. If $\alpha' > 0$ is an actual value, then q could be zero, and for all beams, we have $\alpha_m = \alpha'$. However, if $\alpha' < 0$ is an abnormal value, to guarantee $\alpha_m > 0$, the value of q must be larger than 0, and thus the beams at different subcarriers will be focused on different distances $r_m = \frac{1-\theta_m^2}{2\alpha_m}$. For instance, let the delay parameter α' be $-\frac{2}{d}$, then we have $\alpha_m = \frac{2}{d}(\frac{q}{\eta_m} - 1)$. To guarantee $\alpha_m \geq 0$ is an actual distance ring, the integer q should be larger than η_m. Accordingly, when $f_m \leq f_c$ and $\eta_m = \frac{f_m}{f_c} \leq 1$, then the integer $q = 1$ is enough to make $\alpha_m > 0$ and the beam at f_m is focused on the distance ring $\alpha_m = \frac{2}{d}(\frac{1}{\eta_m} - 1)$. On the other hand, when $f_m > f_c$ and $\eta_m = \frac{f_m}{f_c} > 1$, then the integer $q = 2$ is enough to make $\alpha_m > 0$ and the beam at f_m is focused on the distance ring $\alpha_m = \frac{2}{d}(\frac{2}{\eta_m} - 1)$. As a consequence, the abnormal value of α' is able to introduce and control the beam split effect on the distance domain.

Feature 3: The far-field scenario is a special case of the controllable near-field beam split by setting $\alpha_m = \alpha' = 0$. The far-field scenario assumes the distance is very large, and it can only control the beam split effect on the angle θ_m. By contrast, the controllable near-field beam split effect can adjust the degree of the beam split effect on the angle θ_m and distance r_m jointly. For instance, one can set θ' as an abnormal value and α' as an actual value, then we have $\theta_m = \theta' + 2p/\eta_m$, $\alpha_m = \alpha'$ and $r_m = \frac{1-\theta_m^2}{2\alpha_m} = \frac{1-(\theta'+2p/\eta_m)^2}{2\alpha'}$. Therefore, the beam at frequency f_m is focused on a location satisfying $\left(\frac{1-\theta_m^2}{2r_m}, \theta_m\right) = \left(\alpha', \theta' + \frac{2p}{\eta_m}\right)$, which indicates that the beams are focused on multiple angles in the distance ring α' in the near-field, as shown in Fig. 5 (a). Moreover, we can set θ' as an actual value and α' as an abnormal value, then the beams are focused on multiple distances at the same angle as shown in Fig. 5 (b), satisfying $\left(\frac{1-\theta_m^2}{2r_m}, \theta_m\right) = \left(\alpha' + \frac{2q}{d\eta_m}, \theta'\right)$. As a result, by carefully designing the parameters α' and θ', the beams across the entire band could occupy multiple angles and distances simultaneously, and this property is more flexible than that in the far-field scenario.

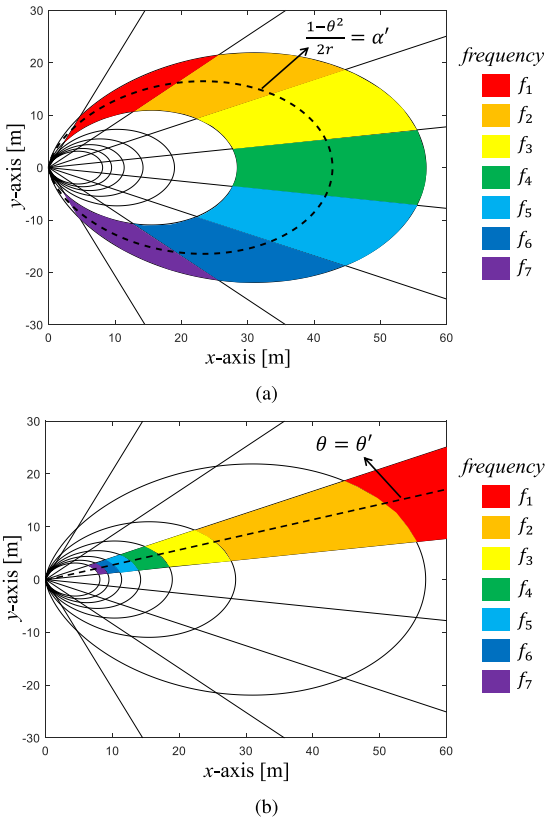

Fig. 5. The schematic diagrams of the near-field rainbow on (a) the angle dimension and (b) the distance dimension.

In conclusion, the mechanism of controllable near-field beam split reveals that TD beamforming can not only mitigate the near-field beam split effect, but also control its degree. TD beamforming allows us to flexibly adjust the covered angle and distance range of beams over multiple frequencies, which is unachievable by PS beamforming. A simple analogy of this effect is the dispersion of white light caused by a prism. Since a prism has different refractive indices for the wideband white light, different frequency components of white light will disperse and eventually produce the rainbow. In our discussion, the function of TD beamforming is similar to that of a prism. Therefore, the controllable near-field beam split effect is also termed as "near-field rainbow" in this paper. By elaborately designing the pattern of the near-field rainbow as shown in Fig. 5, efficient near-field beam management can be accomplished, which will be discussed in the next section.

IV. Near-Field Rainbow Based Beam Training Scheme

In this section, we first introduce the concept of near-field beam training, and point out that the overhead for exhaustive

near-field beam training is unacceptable. To solve this problem, we then propose a wideband beam training algorithm by taking advantage of the near-field rainbow. We also analyze the training overhead and the maximum delay range of the proposed method.

A. Exhaustive Near-Field Beam Training

Beam training is a well-adopted scheme to obtain CSI for current 5G systems [33]. The concept of near-field beam training can be extended from the classical far-field beam training. For the conventional far-field beam training, the spatial angle information θ_0 is desired. The optimal beamsteering vector for a user is selected from a predefined far-field beam codebook through a training procedure between the BS and the user. Generally, each codeword in the far-field codebook determines a unique spatial angle, where the distance is assumed to be very large so that the near-field property is ignored. Therefore, the entire far-field codebook occupies all of the potential angles in the far-field.

Similarly, the near-field beam training desires to obtain the location information (r_0, θ_0) of the dominant path between the BS and the user. The optimal beamfocusing vector is selected from a predefined near-field beam codebook through a training procedure between the BS and the user. Each near-field codeword determines a unique location, and the entire near-field codebook occupies all of the desired angles and distances.

To be more specific, we introduce the procedure of exhaustive near-field beam training realized by TD beamforming. Notice that the procedure below also works well for PS beamforming under narrowband conditions. We define $[\theta_{\min}, \theta_{\max}]$ as the potential range of spatial angle, satisfying $-1 \leq \theta_{\min} \leq \theta_{\max} \leq 1$. Moreover, we assume the minimum distance between the BS and the user is $\rho_{\min}$, so that the potential range of distance is $r \in [\rho_{\min}, +\infty]$ or $\alpha = \frac{1-\theta^2}{2r} \in [0, \alpha_{\max}]$ with $\alpha_{\max} = \frac{1}{2\rho_{\min}}$. Then, multiple angles from $\theta \in [\theta_{\min}, \theta_{\max}]$ and distances from $r \in [\rho_{\min}, +\infty]$ are sampled simultaneously to construct the near-field codebook. It has been proved in [6] that to minimize the largest coherence between two arbitrary codewords of this near-field codebook, the sampled locations could satisfy

$$\theta_u = \theta_{\min} + \frac{u}{U}(\theta_{\max} - \theta_{\min}), \tag{19}$$

$$\alpha_s = \frac{s}{S}\alpha_{\max}, \tag{20}$$

where $u = 0, 1, \cdots, U-1$ and $s = 0, 1, \cdots, S-1$. U denotes the number of sampled angles and S denotes the number of sampled distance rings. More analysis on this near-field codebook, including the near-field beam width and codeword coherence, could be found in our previous study [6]. Notice that when $S = 1$, we have $\alpha_s \equiv 0$, and then the near-field codebook is naturally decayed to the far-field codebook. The exhaustive near-field beam training scheme searches the entire codebook $\{\theta_u\}$ and $\{\alpha_s\}$ to obtain the optimal beamfocusing vector. Apparently, the overhead for exhaustive near-field beam training, i.e., the number of time slots used for beam training, is $T_1 = US$.

In the t-th time slot, where $t = sU + u$ with $t = 0, 1, \cdots, T_1 - 1$, $u = 0, 1, \cdots, U-1$, and $s = 0, 1, \cdots, S-1$, we set the parameters of the TD beamforming as $\theta'_t = \theta_u = \theta_{\min} + \frac{u}{U}(\theta_{\max} - \theta_{\min})$ and $\alpha'_t = \alpha_s = \frac{s}{S}\alpha_{\max}$, and then generate the beamfocusing vector $\mathbf{w}_m(\theta'_t, \alpha'_t)$ according to (11). Since θ'_t and α'_t are actual values, the BS is able to transmit the pilot sequence to the user by the beam focused on the location $(r'_t, \theta'_t) = \left(\frac{1-\theta_u^2}{2\alpha_s}, \theta_u\right)$. So the received signal $y_{m,t}$ in the t-th time slot at f_m is

$$y_{m,t} = \sqrt{P_t}\mathbf{h}_m^T \mathbf{w}_m(\theta'_t, \alpha'_t)x_m + n_m, \tag{21}$$

where $n_m \sim \mathcal{CN}(0, \sigma^2)$ denotes the Gaussian noise, P_t denotes the transmit power, and x_m denotes the transmit pilot satisfying $\|x_m\|^2 = 1$. After T_1 time slots, the estimated physical location $(\hat{r}, \hat{\theta}) = (\frac{1-\hat{\theta}^2}{2\hat{\alpha}}, \hat{\theta})$ corresponding to the largest user received power can be selected from the T_1 measured locations, where,

$$(\hat{\theta}, \hat{\alpha}) = \arg\max_{\theta'_t, \alpha'_t} \sum_{m=1}^{M} \|y_{m,t}\|^2. \tag{22}$$

Finally, a near-field beam $\mathbf{w}_m(\hat{\theta}, \hat{\alpha})$ aligned with the location $(\hat{r}, \hat{\theta})$ can be generated to serve the user, and a near-optimal beamfocusing gain can be achieved.

Nevertheless, since the exhaustive near-field beam training scheme has to search the entire near-field codebook exhaustively, and the scale of the near-field codebook is much larger than that of the far-field codebook, i.e. $US \gg U$, the training overhead is unacceptable in practice. Therefore, a near-field beam training scheme with low training overhead is essential for XL-MIMO systems.

B. Proposed Near-Field Beam Training Scheme

The main reason for the high training overhead of exhaustive near-field beam training is that, only one physical location can be measured in each time slot. By contrast, as we have discussed in Section III-B, TD beamforming is able to generate multiple beams focusing on multiple locations by only one RF chain. By taking advantage of the near-field rainbow, multiple physical locations can be measured simultaneously in each time slot. Inspired by this observation, we propose a near-field rainbow-based beam training method to significantly reduce the training overhead.

Generally, since the spatial resolution of an antenna array on the angle is much higher than that on the distance, the number of sampled angles U is usually much larger than the number of sampled distances S [6]. Thus, the training overhead is mainly determined by the search of angle θ_0. Therefore, the near-field rainbow on the angle dimension, as shown in Fig. 5 (a), is utilized to avoid the exhaustive search of angle, i.e., the angle-related parameters θ' are set as abnormal values, while the distance-related parameters α' can be set as actual values. In other words, the proposed scheme searches the optimal angle in a frequency division manner, and searches the optimal distance ring in a time division manner. The specific procedure of the proposed beam training scheme is illustrated in **Algorithm 1**.

Algorithm 1 Proposed Near-Field Rainbow Based Beam Training Scheme

Require:

Potential angular range $[\theta_{\min}, \theta_{\max}]$, focused angle θ_c at the central frequency, potential distance range $[0, \alpha_{\max}]$, the number of sampled distances S.

Ensure:

Estimated physical location $(\hat{r}, \hat{\theta})$

1: $f_L = f_c - \frac{B}{2}$, $f_H = f_c + \frac{B}{2}$

2: Calculate the abnormal delay parameter: $\theta' = \theta_c - 2\left\lceil \max\left\{f_L(\theta_{\max} - \theta_c), f_H(\theta_c - \theta_{\min})\right\}/B \right\rceil$

3: **for** $t \in \{0, 1, \cdots, S-1\}$ **do**

4: Calculate the normal delay parameter: $\alpha_t' = \frac{t}{S}\alpha_{\max}$

5: Obtain the beamfocusing vector: $[\mathbf{w}_m(\theta', \alpha_t')]_n = \frac{1}{\sqrt{N_t}} e^{-jk_m(nd\theta' - n^2d^2\alpha_t')}$

6: Received signal: $y_{m,t} = \sqrt{P_t}\mathbf{h}_m^T \mathbf{w}_m(\theta', \alpha_t')x_m + n_m$

7: **end for**

8: $(\hat{m}, \hat{t}) = \arg\max_{m,t} \|f_m y_{m,t}\|^2$,

9: $\hat{\theta} = \theta' + (\theta_c - \theta')f_c/f_{\hat{m}}$

10: $\hat{\alpha} = \alpha_{\hat{t}}'$

11: **return** $(\hat{r}, \hat{\theta}) = \left(\frac{1-\hat{\theta}^2}{2\hat{\alpha}}, \hat{\theta}\right)$.

Firstly, in steps 1-2, we desire to design the abnormal parameter $\theta' \notin [-1, 1]$, so that the frequency-dependent angles $\theta_m = \theta' + (2pf_c)/f_m$ across the wideband is able to cover the entire potential angle range $[\theta_{\min}, \theta_{\max}]$, as shown in Fig. 5 (a). To realize this target, we first assume that, at the central frequency f_c, the beam is aligned with the angle $\theta_c = \theta' + 2p$, where θ_c is a predefined spatial angle satisfying $-1 \le \theta_{\min} < \theta_c < \theta_{\max} \le 1$. Then we have

$$\theta' = \theta_c - 2p, \quad p \in \mathbb{Z}. \tag{23}$$

Without loss of generality, we assume the delay parameter $\theta' < -1$, then $p = \frac{\theta_c - \theta'}{2} > \frac{-1-\theta'}{2} > 0$ is a positive integer. In this case, the frequency-dependent angle $\theta_m = \theta' + (2pf_c)/f_m$ is monotonically decreasing with respect to the frequency f_m.

Moreover, since the available bandwidth is B, the lowest frequency and the highest frequency are $f_L = f_c - \frac{B}{2}$ and $f_H = f_c + \frac{B}{2}$, respectively. Therefore, the minimum and maximum values of θ_m are $\theta' + \frac{2pf_c}{f_H}$ and $\theta' + \frac{2pf_c}{f_L}$, respectively. To cover the potential angle range $[\theta_{\min}, \theta_{\max}]$, it should satisfy

$$\theta_{\min} \ge \theta' + (2pf_c)/f_H, \tag{24}$$

$$\theta_{\max} \le \theta' + (2pf_c)/f_L. \tag{25}$$

By solving (23), (24), and (25), one of the solutions to θ' is

$$\theta' = \theta_c - 2\left\lceil \max\left\{f_L(\theta_{\max} - \theta_c), f_H(\theta_c - \theta_{\min})\right\}/B \right\rceil, \tag{26}$$

where $\lceil x \rceil$ denotes the nearest integer greater than or equal to x, and p is given by $p = \frac{\theta_c - \theta'}{2} = \left\lceil \frac{1}{B}\max\left\{f_L(\theta_{\max} - \theta_c), f_H(\theta_c - \theta_{\min})\right\}\right\rceil$.

Then, in step 4, different distance rings are searched in different time slots by adjusting the normal delay parameter α_t'. Similar to the exhaustive near-field beam training scheme, the potential range of distance ring is $\alpha \in [0, \alpha_{\max}]$, and the number of distance rings to be measured is S. Therefore, in the t-th time slot, α_t' is set as $\frac{t}{S}\alpha_{\max}$ with $t = 0, 1, \cdots, S-1$ to measure the beamfocusing gains on the distance ring $\frac{1-\theta^2}{2r} = \alpha_t'$.

As a result, with the parameters α_t' and θ', as shown in Fig. 5 (a), the beams $\mathbf{w}_m(\theta', \alpha_t')$ generated in step 5 by TD beamforming is able to occupy the entire angular range in the distance ring α_t'. Utilizing these beams, in step 6, the received signal $y_{m,t}$ in the t-th time slot at frequency f_m is denoted as

$$\begin{aligned} y_{m,t} &= \sqrt{P_t}\mathbf{h}_m^T \mathbf{w}_m(\theta', \alpha_t')x_m + n_m \\ &= \sqrt{P_t}\sqrt{N_t}\beta_m \mathbf{a}_m^T(\theta_0, r_0)\mathbf{w}_m(\theta', \alpha_t')x_m + n_m \\ &= \sqrt{P_t N_t}\beta_m g_{m,t} x_m + n_m, \end{aligned} \tag{27}$$

where $g_{m,t} = \mathbf{a}_m^T(\theta_0, r_0)\mathbf{w}_m(\theta', \alpha_t')$. The optimal beamfocusing vector is corresponding to the maximum beamfocusing gain $\|g_{m,t}\|^2$. Since $\|x_m\|^2 = 1$ and $n_m \sim \mathcal{CN}(0, \sigma^2)$, the maximum likelihood estimation of $g_{m,t}$ is

$$\hat{g}_{m,t} = \frac{y_{m,t}}{\sqrt{P_t N_t}\beta_m x_m}. \tag{28}$$

Thus, the beamfocusing gain $\|\hat{g}_{m,t}\|^2$ can be estimated as $\|\hat{g}_{m,t}\|^2 = \frac{1}{P_t N_t}\frac{\|y_{m,t}\|^2}{\|\beta_m\|^2}$. Based on the definition of $\|\beta_m\|^2$ in Section II, we have $\|\hat{g}_{m,t}\|^2 = C\|f_m y_{m,t}\|^2$, where C is a constant that is not relevant to f_m. Notice that the proposed beam training scheme does not require the specific value of $\|\beta_m\|^2$. As long as the relationship between β_m and f_m is available, whether quadratic function, exponential function, and so on, the proposed scheme is always valid.

Besides, in step 8, based on the formulation of beamfocusing gain $\|\hat{g}_{m,t}\|^2 = C\|f_m y_{m,t}\|^2$, the label of the optimal beam $\hat{t}$ and $\hat{m}$ is acquired by maximizing $\|\hat{g}_{m,t}\|^2$ over the total S measured distance rings and M subcarriers, where

$$(\hat{m}, \hat{t}) = \arg\max_{m,t} \|f_m y_{m,t}\|^2. \tag{29}$$

Eventually, in steps 9-10, based on the mechanism of the near-field rainbow (16), the estimated spatial location is

$$\hat{\theta} = \theta' + 2p/\eta_{\hat{m}} = \theta' + (\theta_c - \theta')f_c/f_{\hat{m}}, \tag{30}$$

$$\hat{\alpha} = \alpha_{\hat{t}}'. \tag{31}$$

After that, the beam training is completed, and the BS can generate the beamfocusing vector $\mathbf{w}_m(\hat{\theta}, \hat{\alpha})$ to serve the user for data transmission.

The advantage of the proposed near-field rainbow based beam training method is that, the optimal angle is searched out in a frequency division manner. Therefore, the training overhead is only determined by the overhead for searching the optimal distance ring, so it can be significantly reduced. In the next sub-section, we quantitatively analyze the training overheads of the two near-field beam training schemes above.

C. Comparison of the Beam Training Overhead

Beam training overhead refers to the number of time slots used for beam training. It is obvious that, the training overhead of the exhaustive near-field beam training scheme is $T_1 = US$,

while the training overhead of the proposed near-field rainbow based scheme is $T_2 = S$. As discussed in [6], the number of distance rings is generally much less than the number of angles. For instance, if the BS antenna number is $N = 256$, the carrier is $f_c = 60$ GHz, and the minimum distance is $\rho_{\min} = 2$ m, then U is usually set as $U = N = 256$ while S is generally set as 10 [6]. In this case, the training overhead $T_2 = S = 10$ is much less than $T_1 = US = 2560$. Therefore, benefiting from the near-field rainbow, the proposed scheme is able to significantly reduce the pilot overhead for near-field beam training, which will be further verified by simulation results in Section V.

D. Discussion on the Impact of Bandwidth

In addition to the near-field rainbow scheme, we discover that the cost of TD circuits to realize our scheme can be reduced by increasing the system bandwidth. Specifically, the cost of TD circuits is generally proportional to the maximum delay range [21]. In the following discussion, we prove that increasing bandwidth in our scheme can narrow down the maximum delay range.

The delay of the n-th TD circuit is $\tau^{(n)'} = \frac{r^{(n)'}}{c} = n\frac{d\theta'}{c} - n^2\frac{d^2\alpha'}{c}$, where $\alpha' > 0$ and $\theta' = \theta_c - 2\left\lceil \max\left\{f_L(\theta_{\max} - \theta_c), f_H(\theta_c - \theta_{\min})\right\}/B\right\rceil < -1$. In practice, a common delay T is often introduced to each time-delay circuit to ensure that all delays are larger than zero. That is to say, the realistic delay of the n-th antenna is $\bar{\tau}^{(n)'} = \tau^{(n)'} + T = T + n\frac{d\theta'}{c} - n^2\frac{d^2\alpha'}{c}$. To guarantee $\bar{\tau}^{(n)'} > 0$ for every $n \in [-N, N]$, the common delay T could be $T = -\min_n \tau^{(n)'}$. Therefore, the realistic delay becomes $\bar{\tau}^{(n)'} = \tau^{(n)'} - \min_n \tau^{(n)'}$, and the maximum delay range among all TD circuits is

$$\max_n \bar{\tau}^{(n)'} = \max_n \tau^{(n)'} - \min_n \tau^{(n)'}. \tag{32}$$

Now, we prove that the maximum delay range $\max_n \bar{\tau}^{(n)'}$ declines with the increase in bandwidth. For simplicity, define $\xi = \frac{d^2}{c}\alpha' > 0$ and $\gamma = -\frac{d\theta'}{2c} > 0$, so we can rewrite $\tau^{(n)'}$ as $\tau^{(n)'} = -\xi n^2 - 2\gamma n = -\xi(n + \frac{\gamma}{\xi})^2 + \frac{\gamma^2}{\xi}$. Based on the knowledge of quadratic function, it is easy to prove that the extremums of $\tau^{(n)'}$ are

$$\min_n \tau^{(n)'} = \tau^{(N)'} = -\xi N^2 - 2\gamma N, \tag{33}$$

and

$$\max_n \tau^{(n)'} = \begin{cases} \tau^{(-N)'} = -\xi N^2 + 2\gamma N & \text{if } \frac{\gamma}{\xi} \geq N, \\ \tau^{(-\frac{\gamma}{\xi})'} = \frac{\gamma^2}{\xi} & \text{if } \frac{\gamma}{\xi} < N. \end{cases} \tag{34}$$

Therefore, combining (33) and (34), the maximum delay range is presented as

$$\max_n \bar{\tau}^{(n)'} = \begin{cases} 4\gamma N & \text{if } \frac{\gamma}{\xi} \geq N, \\ \frac{\gamma^2}{\xi} + \xi N^2 + 2\gamma N & \text{if } \frac{\gamma}{\xi} < N. \end{cases} \tag{35}$$

It is clear from (35) that if γ and γ^2 are decreasing functions in terms of bandwidth, so is $\max_n \bar{\tau}^{(n)'}$. It is easy to prove that $-\theta' > 0$ is a decreasing function with respect to (w.r.t) bandwidth. Therefore, $\gamma = -\theta'\frac{d}{2c}$ and $\gamma^2 = (-\theta')^2\frac{d^2}{4c^2}$ obviously decline when bandwidth increases. As a consequence, expanding bandwidth is able to narrow down the maximum delay range $\max_n \bar{\tau}^{(n)'}$, so as the cost of time-delay circuits.

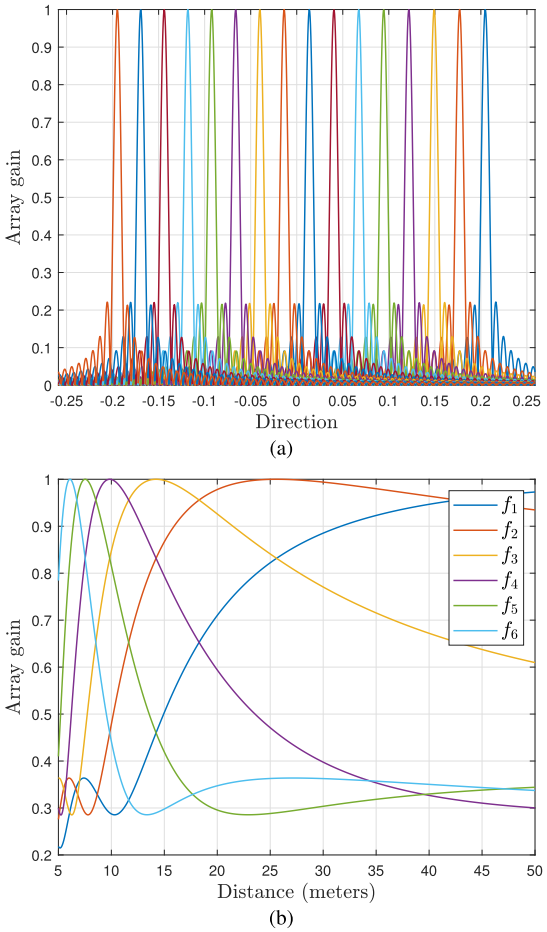

Fig. 6. Near-field rainbow achieved by TD beamforming. In (a), we set $\theta' = -6 \notin [-1, 1]$ and $\alpha' = \frac{1}{20}\text{m}^{-1} > 0$. The array gains at multiple frequencies w.r.t the angle on distance ring α' are evaluated. In (b), we set $\theta' = \frac{\pi}{8} \in [-1, 1]$ and $\alpha' = -\frac{2}{d} < 0$. The array gains at multiple frequencies w.r.t the distance on angle θ' are evaluated.

V. Simulation Results

In this section, simulations are provided to verify the effect of the near-field rainbow and demonstrate the performance of the proposed near-field rainbow based beam training scheme. We consider a wideband XL-MIMO system, where the BS equips an $N_t = 256$-element ULA with TD beamforming architecture. The carrier frequency is $f_c = 60$ GHz, the number of sub-carriers is $M = 2048$, and the bandwidth is $B = 3$ GHz.

A. The Demonstration of Controllable Near-Field Beam Split

Firstly, in Fig. 6, we verify that TD beamforming is able to produce controllable near-field beam split. Specifically, in Fig. 6 (a), the near-field rainbow on the dimension of angle is evaluated. We set the delay parameter θ' as $\theta' = -6 \notin [-1, 1]$ and the parameter α' as $\alpha' = \frac{1}{2r'}$ with $r' = 10$ m. On the distance ring $\alpha' = \frac{1-\theta^2}{2r}$, the array gains at different frequencies w.r.t the angle are shown in Fig. 6 (a). For clarity, only a few frequencies are plotted. The beams over different

frequencies are focused on multiple angles in the distance ring $\alpha' = \frac{1-\theta^2}{2r}$, and cover a given angular range $[-0.2, 0.2]$. Therefore, the near-field rainbow on the angle dimension is verified.

Then, in Fig. 6 (b), the near-field rainbow on the dimension of distance is evaluated. We set the angle θ' as $\theta' = \sin\frac{\pi}{8} \in [-1, 1]$ and the distance ring α' as $\alpha' = -\frac{2}{d} < 0$. In the physical angle θ', array gains at different frequencies w.r.t the distance are shown in Fig. 6(b). For clarity, only a few frequencies are plotted. The beams over different frequencies are focused on multiple distances in the angle θ', which covers the entire distance range. Therefore, the near-field rainbow on the distance dimension is also achievable.

B. Beam Training Performance

In this subsection, the performance of the proposed near-field rainbow based beam training scheme is evaluated. The potential spatial angle range of the user is set as $[\theta_{\min}, \theta_{\max}] = [-\sin\frac{\pi}{3}, \sin\frac{\pi}{3}]$, and the potential distance is set as $[\rho_{\min}, +\infty] = [3\text{ m}, +\infty]$ corresponding to a distance ring α in the range of $[0, \frac{1}{6}\text{m}^{-1}]$. The spatial angle at the center frequency is fixed to $\theta_c = 0$. Then, for the proposed near-field rainbow based scheme, according to (26), the delay parameter θ' is acquired as $\theta' = \xi = -36$ with $p = 18$. Finally, we use the average rate performance to quantify the beam training performance, which is mathematically defined as

$$R = \frac{1}{M}\sum_{m=1}^{M}\log_2\left(1+\frac{P_t}{\sigma^2}\|\mathbf{h}_m^T\mathbf{w}_m\|^2\right) = \frac{1}{M}\sum_{m=1}^{M}\log_2\left(1+\frac{P_t N_t\beta_m^2}{\sigma^2}\|\mathbf{a}_m^T(\theta_0, r_0)\mathbf{w}_m\|^2\right), \quad (36)$$

where $\mathbf{w}_m$ denotes the beamfocusing vector for data transmission searched by beam training and SNR $= \frac{P_t N_t \beta_m^2}{\sigma^2}$ denotes the signal-to-noise ratio. The compared benchmarks are shown below.

- Perfect CSI: The perfect channel $\mathbf{h}_m$ is available at the BS, which is served as the upper bound of average rate performance.
- Far-field rainbow based beam training: This technique is the classical wideband far-field beam training scheme achieved by TD beamforming in [21], where only the optimal angle is searched in a frequency-division manner and the distance information is neglected.
- Near-field hierarchical beam training: This method is the hierarchical beam training scheme designed for reconfigurable intelligence surface (RIS) aided near-field communications [24]. We transform this method to XL-MIMO scenarios for comparison.
- Far-field hierarchical beam training: This approach is the classical hierarchical beam training designed for far-field scenarios [23].
- Exhaustive search: This method is the exhaustive near-field beam training scheme. In the training procedure, we first fix the distance ring α_s and exhaustively search all angles θ_u. Then, we change the distance ring α_s and repeat the above steps until all distance rings and angles are measured.

TABLE I
COMPARISON ON PILOT OVERHEAD

Method	Pilot overhead	Value
Near-field rainbow	S	10
Near-field hierarchical beam training	$\sum_k^K N_x^{(k)} N_y^{(k)}$	200
Near-field exhaustive beam training	US	256
Far-field rainbow	1	1
Far-field hierarchical beam training	$\sum_k^K N^{(k)}$	22

First of all, in Table I, we compare the required pilot overheads for different techniques. We set the number of angle and distance ring samples as $U = 256$ and $S = 10$, respectively. Accordingly, the pilot overheads of the near-field rainbow and near-field exhaustive beam training techniques are $T_2 = S = 10$ and $T_1 = US = 2560$. For near-field hierarchical beam training, [24] proposed a hierarchical near-field codebook, which is composed of K_1 levels of sub-codebooks. Different levels of sub-codebooks have different sampling ranges and scales. The k-th level sub-codebook divides the k-th sampling range in the x-y plane into $N_x^{(k)} N_y^{(k)}$ grids, where $N_x^{(k)}$ and $N_y^{(k)}$ represent the number of grids on the x-axis and y-axis, respectively. In our simulations, we set $K_1 = 2$ and $N_x^{(k)} = N_y^{(k)} = 10$ for $k = 1, 2$. Therefore, the overall pilot overhead is 200. The far-field hierarchical beam training is carried out similarly, while it divides the angle space, instead of the x-y plane, into $N^{(k)}$ grids in the k-th level. In our simulations, we set $K_2 = 3$, $N^{(1)} = N^{(2)} = 8$, and $N^{(3)} = 6$, which gives rise to a pilot overhead of 22. Regarding the far-field rainbow technique, as it utilizes TD beamforming to search the optimal angle while neglecting the distance information, it only needs 1 pilot overhead.

Fig. 7 illustrates the average rate performance against the training overhead. The training overhead is increasing from 0 to $US = 2560$. The SNR is set as 10 dB. 10^3 realizations of the user location are generated for Monte Carlo simulations, where $\theta_0 \sim \mathcal{U}(-\sin\frac{\pi}{3}, \sin\frac{\pi}{3})$ and $r_0 \sim \mathcal{U}(3\text{meters}, 30\text{meters})$. In each time slot, we utilize the optimal beamforming vector we have searched in previous time slots to serve the user. Specifically, the training overhead of the two far-field schemes are both very low, e.g., 22 overhead for the far-field hierarchical technique and only one overhead for the far-field rainbow based technique. However, since the far-field approaches only consider the angle information while ignoring the distance information, their average rate performance is not satisfactory. Besides, to achieve a satisfactory average rate, the training overhead of the near-field hierarchical scheme and exhaustive scheme will be very high, e.g., 200 overhead for the near-field hierarchical scheme and more than 1000 for the exhaustive scheme. By contrast, the proposed near-field rainbow based beam training scheme enjoys a much higher average rate performance with very low overhead. This is thanks to two factors: 1) both the angle and distance information are considered, 2) the near-field rainbow effect is exploited to avoid the exhaustive search for the angle information. Actually, the proposed scheme has

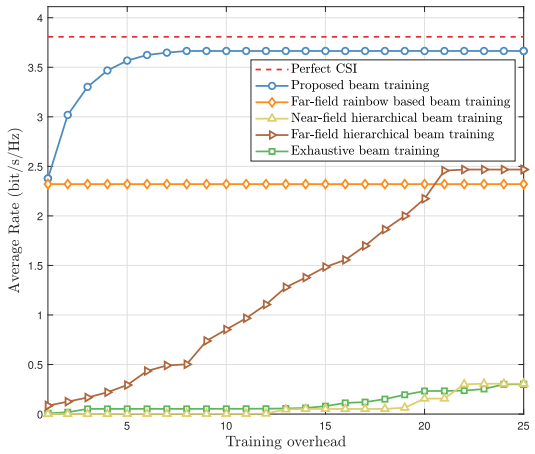

(a)

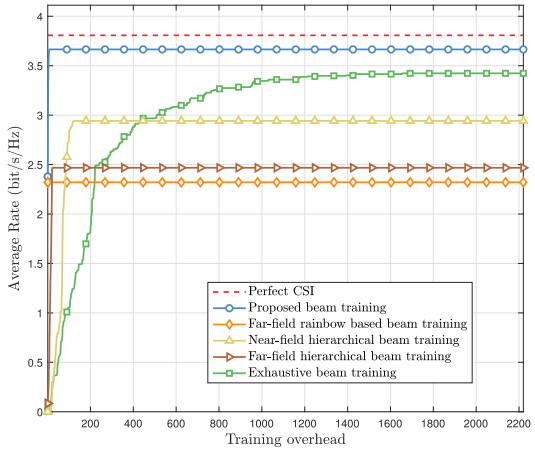

(b)

Fig. 7. Average rate performance vs. training overhead.

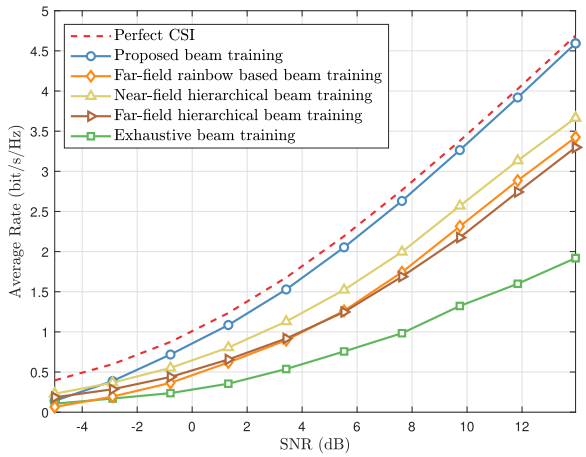

Fig. 8. Average rate performance vs. SNR.

already achieved 96% of the average rate benchmark with only 8 training overhead.

Fig. 8 presents the impact of SNR on different beam training schemes, where SNR is growing from -5 dB to 15 dB. For a fair comparison, we constrain the maximum training overhead $T_{\max}$ for all considered methods as $T_{\max} = 256$. The other simulation settings are the same as those in Fig. 7. It is clear from Fig. 8 that, as long as SNR is larger

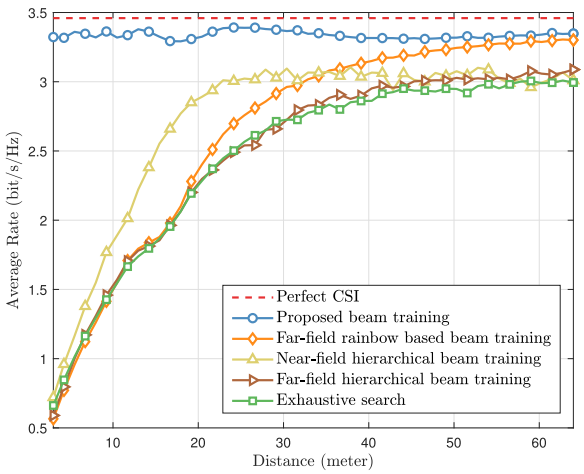

Fig. 9. Average rate performance vs. distance.

than -2 dB, the proposed scheme outperforms all existing far-field and near-field beam training schemes and is able to achieve a near-optimal achievable average rate performance. When SNR $= 10$ dB, around 25% improvement in average rate is accomplished by the proposed technique compared to existing approaches. In addition, we can observe that the proposed technique is comparable to the other schemes under low SNR regime. This is because our scheme uses beams with different frequencies to search different locations, which differs from the exhaustive beam training approach (22) which accumulates the power from all frequencies to combat noise. Therefore, our scheme might be vulnerable to noise, especially under low SNR regime. A possible solution is to divide subcarriers into several groups. By meticulously designing the TD parameters, beams within the same group are focused on the same location while beams belonging to different groups are separated from each other. In this way, we can not only improve the beam training efficiency but also accumulate the signal power from frequencies in the same group to combat noise. In fact, a similar grouping technique has been studied in the literature [21] on far-field wideband beam training. How to apply this grouping technique to near-field rainbow is a future research direction.

In Fig. 9, we illustrate the average rate performance against the distance. Here, the distance r_0 between the user and BS is gradually increasing from 3 meters to 60 meters. The parameters are set as follows: SNR $= 10$ dB, $T_{\max} = 256$, $\theta_0 \in \mathcal{U}(-\sin\frac{\pi}{6}, \sin\frac{\pi}{6})$. The other simulation settings are the same as those in Fig. 8. The impact of near-field propagation on the beam training performance is clear in Fig. 9. For the far-field schemes, with the decrease of distance, near-field propagation becomes dominant and thus the average rate of these far-field schemes rapidly deteriorates. As for the degradation of the exhaustive scheme, since the maximum training overhead is limited to 256, this scheme is hard to search the locations in the near-field. Moreover, although the near-field hierarchical beam training scheme is able to slightly alleviate the average rate loss, its performance is unacceptable when the distance is less than 20 meters. By contrast, since the proposed scheme is able to search the optimal angle

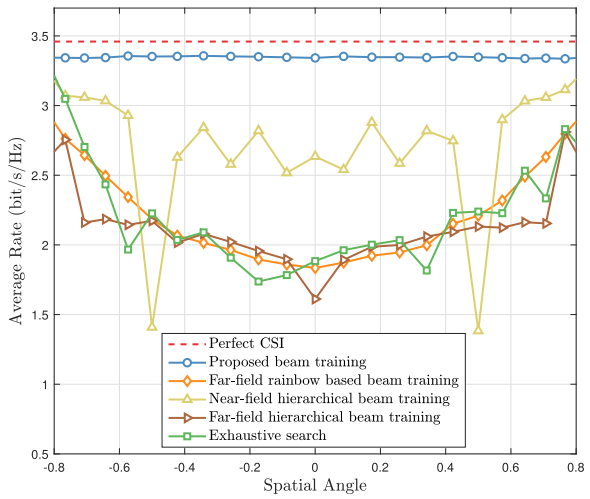

Fig. 10. Average rate performance vs. angle.

and distance with very low pilot overhead by exploiting the near-field rainbow, its performance is robust to all considered distances, whether in the near-field or in the far-field.

Fig. 10 shows the average rate performance against the angle θ_0. Here, the angle θ_0 is gradually increasing from $-\sin\frac{\pi}{3}$ to $\sin\frac{\pi}{3}$ and the distance r_0 is randomly generated from $r_0 \sim \mathcal{U}(3 \text{ meters}, 30 \text{ meters})$. The other simulation settings are the same as those in Fig. 9. Notice that although the distance r_0 is fixed, the distance ring $\alpha_0 = \frac{1-\theta_0^2}{2r_0}$ still varies with the angle θ_0. For the far-field schemes, their performance is severely degraded when the angle θ_0 is around zero. This is because the near-field property is more significant when the angle is around zero, which has been proved in [5]. Moreover, there exists severe fluctuation for the near-field hierarchical beam training scheme. This is because the near-field hierarchical scheme proposed in [24] creates the near-field codebook by uniformly sampling the codeword in the cartesian coordinates. It has been indicated in [6] that this kind of codebook cannot realize satisfactory beam training performance in the entire near-field environment. By contrast, the proposed scheme achieves a near-optimal average rate for all considered angles.

VI. Conclusion

This paper investigated the wideband near-field beam training for XL-MIMO systems. The mechanism of the near-field rainbow is revealed, i.e., TD beamforming can flexibly control the degree of the near-field beam split effect. Then, a near-field rainbow based beam training technique was proposed, which searches the optimal angle in a frequency-division manner and the optimal distance in a time-division manner. Simulation results verified that: 1) the beams generated by TD beamforming over mutiple frequencies can cover multiple angles and distances; 2) our near-field rainbow based scheme can achieve a near-optimal average rate with significantly reduced training overhead; 3) the performance of our scheme is robust to the distance and angle. This paper unveiled that although the near-field beam split effect induces a severe beamfocusing gain loss, it also provides a new possibility to realize fast near-field CSI acquisition. For future works, we may investigate the near-field beam split effect in other beamforming architectures, such as delay-phase precoding [14] and extremely large lens antenna arrays [34].

Appendix A. The Periodicity of $G(x, y)$

$G(x, y)$ is a periodic function against the vector variable (x, y) with period $(\frac{2\pi}{d}, \frac{2\pi}{d^2})$. Specifically, for any integers $p \in \mathbb{Z}$ and $q \in \mathbb{Z}$, $G\left(x - \frac{2p\pi}{d}, y - \frac{2q\pi}{d^2}\right)$ can be presented as

$$\frac{1}{N_t}\left|\sum_{n=-N}^{N} e^{jnd(x-\frac{2p\pi}{d})-jn^2d^2(y-\frac{2q\pi}{d^2})}\right| = \frac{1}{N_t}\left|\sum_{n=-N}^{N} e^{jndx-jn^2d^2y}e^{j2\pi n(qn-p)}\right|. \quad (37)$$

Since $2\pi n(qn-p)$ is an integer multiple of 2π, we have $e^{j2\pi n(qn-p)} = 1$. Therefore, we arrive at

$$G\left(x - \frac{2p\pi}{d}, y - \frac{2q\pi}{d^2}\right) = \frac{1}{N_t}\left|\sum_{n=-N}^{N} e^{jndx-jn^2d^2y}\right| = G(x, y). \quad (38)$$

As a result, the periodicity of function $G(x, y)$ is proved.

References

[1] E. D. Carvalho, A. Ali, A. Amiri, M. Angjelichinoski, and R. W. Heath, "Non-stationarities in extra-large-scale massive MIMO," *IEEE Wireless Commun.*, vol. 27, no. 4, pp. 74–80, Aug. 2020.
[2] P. Frenger, J. Hederen, M. Hessler, and G. Interdonato, "Improved antenna arrangement for distributed massive MIMO," U.S. Patent 103 897, Jun. 14, 2018. [Online]. Available: patentscope.wipo.int/search/en/WO2018103897
[3] T. S. Rappaport et al., "Wireless communications and applications above 100 GHz: Opportunities and challenges for 6G and beyond," *IEEE Access*, vol. 7, pp. 78729–78757, 2019.
[4] H. Elayan, O. Amin, B. Shihada, R. M. Shubair, and M.-S. Alouini, "Terahertz band: The last piece of RF spectrum puzzle for communication systems," *IEEE Open J. Commun. Soc.*, vol. 1, pp. 1–32, 2020.
[5] M. Cui, L. Dai, R. Schober, and L. Hanzo, "Near-field wideband beamforming for extremely large antenna arrays," 2021, *arXiv:2109.10054*.
[6] M. Cui and L. Dai, "Channel estimation for extremely large-scale MIMO: Far-field or near-field?" *IEEE Trans. Commun.*, vol. 70, no. 4, pp. 2663–2677, Apr. 2022.
[7] H. Zhang, N. Shlezinger, F. Guidi, D. Dardari, M. F. Imani, and Y. C. Eldar, "Beam focusing for near-field multiuser MIMO communications," *IEEE Trans. Wireless Commun.*, vol. 21, no. 9, pp. 7476–7490, Sep. 2022.
[8] K. T. Selvan and R. Janaswamy, "Fraunhofer and Fresnel distances: Unified derivation for aperture antennas," *IEEE Antennas Propag. Mag.*, vol. 59, no. 4, pp. 12–15, Aug. 2017.
[9] D. Headland, Y. Monnai, D. Abbott, C. Fumeaux, and W. Withayachumnankul, "Tutorial: Terahertz beamforming, from concepts to realizations," *APL Photon.*, vol. 3, no. 5, May 2018, Art. no. 051101.
[10] Z. Wu, M. Cui, and L. Dai, "Multiple access for near-field communications: SDMA or LDMA?" 2022, *arXiv:2208.06349*.
[11] M. Cui, Z. Wu, Y. Lu, X. Wei, and L. Dai, "Near-field communications for 6G: Fundamentals, challenges, potentials, and future directions," *IEEE Commun. Mag.*, early access, Sep. 26, 2022, doi: 10.1109/MCOM.004.2200136.
[12] R. J. Mailloux, *Phased Array Antenna Handbook*. Norwood, MA, USA: Artech House, 2005.
[13] T. S. Rappaport et al., "Millimeter wave mobile communications for 5G cellular: It will work!" *IEEE Access*, vol. 1, pp. 335–349, 2013.
[14] L. Dai, J. Tan, Z. Chen, and H. V. Poor, "Delay-phase precoding for wideband THz massive MIMO," *IEEE Trans. Wireless Commun.*, vol. 21, no. 9, pp. 7271–7286, Sep. 2022.

[15] B. Wang, F. Gao, S. Jin, H. Lin, and G. Y. Li, "Spatial- and frequency-wideband effects in millimeter-wave massive MIMO systems," *IEEE Trans. Signal Process.*, vol. 66, no. 13, pp. 3393–3406, May 2018.
[16] H. Hashemi, T.-S. Chu, and J. Roderick, "Integrated true-time-delay-based ultra-wideband array processing," *IEEE Commun. Mag.*, vol. 46, no. 9, pp. 162–172, Sep. 2008.
[17] E. Ghaderi, A. S. Ramani, A. A. Rahimi, D. Heo, S. Shekhar, and S. Gupta, "An integrated discrete-time delay-compensating technique for large-array beamformers," *IEEE Trans. Circuits Syst. I, Reg. Papers*, vol. 66, no. 9, pp. 3296–3306, Sep. 2019.
[18] C. Lin, G. Y. Li, and L. Wang, "Subarray-based coordinated beamforming training for mmWave and sub-THz communications," *IEEE J. Sel. Areas Commun.*, vol. 35, no. 9, pp. 2115–2126, Sep. 2017.
[19] A. Liao et al., "Terahertz ultra-massive MIMO-based aeronautical communications in space-air-ground integrated networks," *IEEE J. Sel. Areas Commun.*, vol. 39, no. 6, pp. 1741–1767, Jun. 2021.
[20] H. Yan, V. Boljanovic, and D. Cabric, "Wideband millimeter-wave beam training with true-time-delay array architecture," in *Proc. 53rd Asilomar Conf. Signals, Syst., Comput.*, Nov. 2019, pp. 1447–1452.
[21] V. Boljanovic et al., "Fast beam training with true-time-delay arrays in wideband millimeter-wave systems," *IEEE Trans. Circuits Syst. I, Reg. Papers, Reg. Papers*, vol. 68, no. 4, pp. 1727–1739, Apr. 2021.
[22] J. Tan and L. Dai, "Wideband beam tracking in THz massive MIMO systems," *IEEE J. Sel. Areas Commun.*, vol. 39, no. 6, pp. 1693–1710, Jun. 2021.
[23] S. Noh, M. D. Zoltowski, and D. J. Love, "Multi-resolution codebook and adaptive beamforming sequence design for millimeter wave beam alignment," *IEEE Trans. Wireless Commun.*, vol. 16, no. 9, pp. 5689–5701, Sep. 2017.
[24] X. Wei, L. Dai, Y. Zhao, G. Yu, and X. Duan, "Codebook design and beam training for extremely large-scale RIS: Far-field or near-field?" *China Commun.*, vol. 19, no. 6, pp. 193–204, Jun. 2022.
[25] Y. Zhu, H. Guo, and V. K. N. Lau, "Bayesian channel estimation in multi-user massive MIMO with extremely large antenna array," *IEEE Trans. Signal Process.*, vol. 69, pp. 5463–5478, 2021.
[26] Z. Zhou, X. Gao, J. Fang, and Z. Chen, "Spherical wave channel and analysis for large linear array in LoS conditions," in *Proc. IEEE Globecom Workshops (GC Wkshps)*, Dec. 2015, pp. 1–6.
[27] W. Tang et al., "Wireless communications with reconfigurable intelligent surface: Path loss modeling and experimental measurement," *IEEE Trans. Wireless Commun.*, vol. 20, no. 1, pp. 421–439, Jan. 2021.
[28] J. Sherman, "Properties of focused apertures in the Fresnel region," *IRE Trans. Antennas Propag.*, vol. 10, no. 4, pp. 399–408, Jul. 1962.
[29] D. Tse and P. Viswanath, *Fundamentals of Wireless Communication*. Cambridge, U.K.: Cambridge Univ. Press, 2005.
[30] L. Yan, Y. Chen, C. Han, and J. Yuan, "Joint inter-path and intra-path multiplexing for terahertz widely-spaced multi-subarray hybrid beamforming systems," *IEEE Trans. Commun.*, vol. 70, no. 2, pp. 1391–1406, Feb. 2022.
[31] H. Zhang, N. Shlezinger, F. Guidi, D. Dardari, and Y. C. Eldar, "6G wireless communications: From far-field beam steering to near-field beam focusing," 2022, *arXiv:2203.13035*.
[32] T.-S. Chu and H. Hashemi, "A true time-delay-based bandpass multi-beam array at mm-waves supporting instantaneously wide bandwidths," in *Proc. IEEE Int. Solid-State Circuits Conf. (ISSCC)*, Feb. 2010, pp. 38–39.
[33] W. Wu, D. Liu, X. Hou, and M. Liu, "Low-complexity beam training for 5G millimeter-wave massive MIMO systems," *IEEE Trans. Veh. Technol.*, vol. 69, no. 1, pp. 361–376, Jan. 2020.
[34] J. Yang, Y. Zeng, S. Jin, C.-K. Wen, and P. Xu, "Communication and localization with extremely large lens antenna array," *IEEE Trans. Wireless Commun.*, vol. 20, no. 5, pp. 3031–3048, May 2021.

Mingyao Cui received the B.E. degree in electronic engineering from Tsinghua University, Beijing, China, in 2020, where he is currently pursuing the M.S. degree in electronic engineering. His research interests include massive MIMO, millimeter-wave communications, and near-field communications. He received the IEEE ICC Oustanding Demo Award and the National Scholarship in 2022.

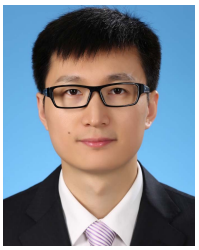

Linglong Dai received the B.S. degree from Zhejiang University, Hangzhou, China, in 2003, the M.S. degree from the China Academy of Telecommunications Technology, Beijing, China, in 2006, and the Ph.D. degree from Tsinghua University, Beijing, in 2011. From 2011 to 2013, he was a Post-Doctoral Researcher at the Department of Electronic Engineering, Tsinghua University, and an Assistant Professor from 2013 to 2016, where he has been an Associate Professor, since 2016. His current research interests include massive MIMO, reconfigurable intelligent surface (RIS), millimeter-wave and Terahertz communications, wireless AI, and electromagnetic information theory. He received the National Natural Science Foundation of China for Outstanding Young Scholars in 2017, the IEEE ComSoc Leonard G. Abraham Prize in 2020, and the IEEE ComSoc Stephen O. Rice Prize in 2022.

Zhaocheng Wang received the B.S., M.S., and Ph.D. degrees from Tsinghua University in 1991, 1993, and 1996, respectively. From 1996 to 1997, he was a Post-Doctoral Fellow with Nanyang Technological University, Singapore. From 1997 to 1999, he was a Research Engineer/Senior Engineer with OKI Techno Centre Pte. Ltd., Singapore. From 1999 to 2009, he was a Senior Engineer/Principal Engineer with Sony Deutschland GmbH, Germany. Since 2009, he has been a Professor with the Department of Electronic Engineering, Tsinghua University, where he is currently the Director of the Broadband Communication Key Laboratory, BNRist. His research interests include mmWave communications, optical wireless communications, and AI empowered wireless communications. He was a recipient of the 2016 IEEE Scott Helt Memorial Award, the 2016 IET Premium Award, the 2016 National Award for Science and Technology Progress (First Prize), the ICC2017 Best Paper Award, the 2018 IEEE ComSoc Asia-Pacific Outstanding Paper Award, and the 2020 IEEE ComSoc Leonard G. Abraham Prize.

Shidong Zhou received the bachelor's and master's degrees from Southeast University in 1991 and 1994, respectively, and the Ph.D. degree from Tsinghua University, Beijing, China, in 1998. He is currently a Professor with the Department of Electronic Engineering, Tsinghua University. He involved in Program for New Century Excellent Talents in University 2005 (Ministry of Education). His research interests include wireless transmission techniques, including distributed wireless communication systems, channel sounding and modeling, coordination of communication, control and computing, and application in future mobile communications. He received the Special Award of 2016 National Prize for Progress in Science and Technology.

Ning Ge received the B.S. and Ph.D. degrees from Tsinghua University, China, in 1993 and 1997, respectively. From 1998 to 2000, he was at the Development of ATM switch fabric ASIC in ADC Telecommunications, Dallas. Since 2000, he has been with the Department of Electronics Engineering, Tsinghua University. From 2000 to 2006, he was the Chief Scientist of Tsinghua Huahuan Company. His current research interests include ASIC design, short range wireless communication, and wireless communications. He has undertaken many national research projects, such as the 973 program, the 863 plans, and the national major project. He is also a Senior Member of CIC and CIE. He received the First Prize of the Science and Technology Award of the Communication Society and the First Prize of Wu Wenjun's Artificial Intelligence Science and Technology Progress Award.